Semi-empirical models to describe the absorption of liquid water in natural stones employed in built heritage before and after the application of water repellent treatments

Marco Roveri[a,*], Sara Goidanich[a], Giovanni Dotelli[a] and Lucia Toniolo[a]

[a] Dipartimento di Chimica, Materiali e Ingegneria Chimica "G. Natta", Politecnico di Milano, Piazza Leonardo da Vinci 32, 20133 Milano, Italy

* Corresponding author. Tel.: +39 0223993143
E-mail address: marco.roveri@polimi.it (Marco Roveri)

Abstract
This study aims at validating an easily implementable and effective methodology to simulate the capillary imbibition rate of porous building materials, with special attention to stones employed in historical architecture. Two models selected from the literature are discussed from both a theoretical and practical viewpoint and their effectiveness in describing the imbibition process is evaluated on a large set of water absorption data of four different natural stones. It is shown that these models can be used in a predictive way to calculate the sorptivity of stones with fairly good approximation. Furthermore, they may represent a useful tool for the study of porous materials of built heritage, since, contrary to standard tests for sorptivity determination, they only require small samples to determine the pore size distribution and the maximum water saturation of the investigated materials. Finally, it is shown that the same models can also be used to simulate the reduction in water absorption after the application of water-repellent products, affording some insight into the protection mechanism and the criteria that determine the performance of protective treatments.

Keywords
stone; cultural heritage; modelling; water absorption; capillary imbibition; protective treatments

Highlights
- A modelling approach for predicting the sorptivity of porous stones from microstructure is validated on a large set of water absorption data of different natural stones.
- The proposed methodology only requires minimal sampling of the investigated materials, being tailored for the study of porous building materials used in architectural heritage.
- A mechanistic model of pore hydrophobization simulates the effect of protective treatments on the capillary absorption of stones.

1. Introduction
For porous building materials, such as stone, mortar, brick and concrete, capillary imbibition phenomena are relevant in many respects. Several weathering processes that affect these materials, such as salt-crystallization [1], freezing-thawing cycles [2], dissolution of soluble fractions [3], and swelling of clays [4] owe their onset to liquid water penetration, either in the form of meteoric precipitation or groundwater moisture infiltration. Moreover, as a consequence of microstructural modifications induced by the above mentioned processes, increasing weathering levels often result in increasing imbibition rates [5]. Capillary absorption measurements not only provide a fundamental indication for monitoring the progress of materials degradation but also critical parameters for evaluating the efficacy of protective treatments applied to stone materials with the aim of preventing or reducing water penetration [6].

According to European Standard EN 15801 [7], laboratory measurements of capillary absorption must be performed on samples with a regular geometry (prisms or cylinders), which represents a considerable limitation in the study of heritage materials. Indeed, whilst these tests are quite easy to perform on freshly quarried specimens, they can hardly be carried out on samples collected from buildings, subjected to specific regulations for cultural heritage safeguard [8]. Another limitation is encountered in the testing of protective treatments. Experience in the field of building materials indicates that the protective performance cannot be explained unless the complex system resulting from the interaction of stones with treatments is taken into account [9]. Water-repellent products, particularly if relying on a sol-gel reaction to create an effective

barrier against water penetration, have a complex interaction with porous materials, which determines, e.g., their penetration, reactivity and, ultimately, ability to ensure a homogeneous pore hydrophobization [6,10]. Due to this fact, the laboratory evaluation of protective performance, which includes, among other tests, the measurement of water absorption before and after the application of the treatments, often requires that a considerable number of products should be tested in order to select the most appropriate one [9], thus involving time and material-consuming experimental procedures. In both these regards, predictive models of capillary imbibition would be particularly helpful to simulate laboratory tests, not only giving responses about the hydric behaviour of weathered stones in heritage buildings but also rationalizing their interaction with protective treatments and indicating which products, among the many available, may be best suited to the protection of a given substrate.

Several works over the last 40 years have pursued, for a variety of interests and applications, the aim of modelling the imbibition of fluids into different porous media. Theoretical interest in capillary phenomena, originating from research fields such as soil science, hydrogeology and petroleum engineering, led to formulate the continuum-based theory of unsaturated flow, on which the modelling of fluid dynamics in large domains such as aquifers is based [11,12]. Later on, the topic of capillary imbibition also became of interest to materials science, where however a fundamentally different modelling approach was adopted with respect to the above-mentioned fields. Materials science is generally concerned with small material domains and regards them as systems with a discrete internal structure rather than continua. Accordingly, many models describing capillary imbibition or physical properties in rocks and other porous materials use microstructural data to make assumptions on the structure and topology of the pore space [13-15] and then adopt a suitable mathematical description of the flow or other properties of interest inside this space. The simplest and oldest of such models is no doubt the so-called “capillary bundle model” of fluid flow, which is based on the assumption that porous solids may be described as an ensemble of parallel cylindrical capillaries [16]. More complex instances include pore network models of capillary pressure and fluid flow [17,18] and fractal models describing properties such as pore shape and tortuosity [19,20] or simulating the pore size distribution [8,21]. The development of digital tools during the last 20 years has substantially widened the perspectives of computation, also opening the way to advanced imaging techniques of the internal structure of porous materials such as Computed Tomography (CT) [22,23].

Nevertheless, given the high complexity and heterogeneity of porous materials, models developed for a specific class of materials are often found to be ineffective on others. Moreover, not all modelling procedures comply with the specific needs of cultural heritage research. First, they should rely on characterization techniques that are non-invasive or only require the sampling of small fragments to acquire the necessary preliminary information on the materials microstructure [8,22]. Secondly, they should be easily implementable, helping to understand phenomena and providing support to the experimental work, while remaining accessible to people with no strong background in computational tools.

Another challenge is posed by the prediction of the effect of water-repellent treatments on the water absorption behaviour of stones. These treatments, which nowadays mainly consist of silicon-based compounds, i.e., alkylsilanes or siloxanes, penetrate into the pores of stone materials, covering grain boundaries with a thin protective layer that is able to hydrophobize the stone pores up to few millimetres from the surface [24,25] without causing relevant alterations of the deeper microstructure. Most of the protective performance relies on the efficiency by which treatments modify the water/stone interface, adhering to the stone grains and adapting to their surface morphology, while the penetration depth was shown to have a looser correlation to the performance [9]. However, acquiring direct evidence of the modification of this interface is a difficult task. Contact angle measurements are generally used with this aim, yet the information they provide is more related to an instantaneous water-repellent effect, which also depends on intrinsic textural parameters such as surface roughness. Mercury Intrusion Porosimetry (MIP) has been used in some cases to quantify the changes in pore size distribution due to consolidant and protective treatments with good penetration ability [26] and, accordingly, to predict the decrease in stone permeability [27], but the results of this analysis alone can be misleading [28] and the suitability of the technique to describe changes in porosity due to consolidation has been questioned [29]. As regards microscopy techniques, scanning electron microscopy (SEM) and Energy Dispersive X-Ray Spectroscopy (EDS) can be used to characterize, morphologically and chemically, the modification of the stone surface, but they are much less effective in detecting the product distribution inside pores from the analysis of stone cross sections, while the potential of μ-CT scanning, which is able to visualize the 3D structure of the pore network, is limited by spatial resolution and low contrast between silicon-based products and stone minerals [24].

In this research, the issue of modelling the water absorption rate in porous materials of historical architecture was handled by selecting, upon a survey of literature, two existing models of capillary imbibition, and, after a theoretical discussion, evaluating their effectiveness against a large set of data of four different porous rocks, chosen as reference substrates and characterized by different petrological features. These models are based on two alternative configurations of the pore space, namely the capillary bundle and the pore network model. Both of them use MIP to gain knowledge of the stone microstructure and are potentially of great interest for heritage materials, as the mercury intrusion technique only requires very small samples (about 1 cm^3), which can easily be collected from historical buildings and monuments.

Then, a simple mechanistic model of pore hydrophobization was devised with the aim of simulating the effect of protective treatments and its validity was checked by adapting the two models of capillary imbibition and using them to describe the reduction in water absorption in the four stones after the application of two silicon-based water repellent treatments.

The aims of the research are, therefore: (i) to discuss from a theoretical viewpoint two different literature models that describe spontaneous imbibition in porous materials; (ii) to evaluate these models in order to validate an easily implementable and effective methodology to simulate the capillary imbibition rate of building materials, with possible application to heritage stones; (iii) to extend such methodology in order to simulate the effect of protective treatments, providing some insight into the protection mechanism and the criteria that determine the performance of these treatments.

The research framework was provided by the EU H2020 Nano-Cathedral project [30], which concerned the development and testing of innovative consolidant and protective treatments, both on laboratory scale and in situ, on a variety of stone substrates employed in European Middle-Age cathedrals.

2. **Modelling approach**

2.1. Modelling of capillary imbibition

The kinetics of capillary imbibition was described within the theoretical framework given by Lucas-Washburn (L-W) equation [16,31]

$$L(t) = \left(\frac{d\gamma \cos\theta}{4\mu} t\right)^{1/2} \quad (1)$$

where $L(t)$ indicates the position of the liquid meniscus at elapsed time t along the pore path, d is capillary diameter, γ and μ are the surface tension and viscosity of the liquid, respectively, and θ is the contact angle formed between the liquid meniscus and the capillary wall, which was set equal to 0 in agreement with literature [14]. The approximations made by eq. 1, including the disregard of inertia and gravity contributions to the flow dynamics, have been shown to involve no significant loss of predictive accuracy if the capillary size is in the order of 100 μm or less [32,33] (as it is the case of pores practically contributing to the process of spontaneous imbibition in porous rocks [34] and if its length is small compared to the equilibrium height reached by the fluid [35], which is by far verified by stone specimens with 2 cm height. Also, the possible effects deriving from the use of static instead of dynamic contact angles were shown to be negligible for liquids having the viscosity and surface tension of water [36]. The effect of the air co-current flow in single open capillaries was overlooked [37], because air and water viscosity differ by nearly two orders of magnitude. However, the presence of air in the pore space resulting in incomplete saturation of the medium was taken into account by measuring maximum water saturation (S_{wf}) and, in accordance with literature [38-40], this parameter was included in the modelling of the imbibition rate.

L-W equation was applied to two different pore space configurations: (i) capillary bundle model and (ii) pore network model.

2.1.1. Capillary bundle model

The capillary bundle model [16] was set up assuming independent pores with an upright orientation and a circular cross section (supposed to be constant over the entire pore length). As unique deviation from geometrical ideality, pores were allowed to display non-straight paths and tortuosity factors were accordingly introduced. For all pores of a given diameter d_i, tortuosity (τ_i) is defined by

$$\tau_i = \frac{L_i}{L_0} \quad (2)$$

where L_i is the linearized pore length and L_0 is the minimum distance between its ends. In the case of stone specimens such as are those used in water absorption measurements, this distance can be set equal to the macroscopic height of the specimens.

Supposing that pores have an average length L_{av}, eq. 2 can also be used to define an average tortuosity (τ_{av}). Several empirical relationships between the latter and the open porosity (ϕ) have been proposed for porous materials [59-61]. In the present study, the widely accepted equation by Comiti and Renaud [45]

$$\tau_{av} = 1 - F \ln \phi \quad (3)$$

was used, where F is an empirical constant with values usually falling in the range between 0.5 and 1 [46]. A recent study where tortuosity data of a wide range of porous materials with different porosity were fitted to eq. 3 found that a value of 0.60 yields the best regression [46], hence this was the value adopted by Cai et al. [40] and used in the present research.

Tortuosity factors τ_i were calculated by using the model proposed by Yu et al. [20,41-44], which involves fractal-geometry considerations. The main assumption of the model is that tortuosity can be described through a self-similarity relationship, the scale thereof being dictated by the pore size: smaller pores are supposed to display greater tortuosity and so to be longer than larger pores. In particular, the fractal scaling law

$$L_i = {d_i}^{1-D_T} {L_0}^{D_T} \quad (4)$$

is used to correlate the pore length L_i to the diameter d_i. D_T in eq. 4 is the fractal dimension of tortuosity, which can be expressed as [20]

$$D_T = 1 + \frac{ln\, \tau_{av}}{ln \frac{L_0}{d_{av}}} \quad (5)$$

by combining eqs. 2 and 4 and substituting τ_{av} for τ_i and d_{av} (i.e., average pore diameter) for d_i. Yu's model also describes the pore size distribution under fractal terms. Without entering too many details, the model correlates the L_0/d_{av} term in eq. 5 to the fractal dimension of the pores (D_f), which in turn depends on the open porosity and the pore size range of the material, i.e., the maximum and minimum pore diameters [20]. As regards D_f, it is worth remembering that in a capillary bundle configuration, where pores have constant cross section and share the same orientation in space, its values can range between 1 and 2.

The multiplicity n_i of the i-th pore size class, i.e., the number of pores having the same diameter d_i , can be obtained from the specific volume V_i (measured through mercury porosimetry) by applying the simple identity

$$n_i = \frac{4V_i}{\pi {d_i}^2 L_i} \cdot \frac{V_A \cdot \phi}{\sum V_i} \quad (6)$$

where $\frac{V_A \cdot \phi}{\sum V_i}$ is the scale factor to convert V_i into its corresponding value relative to the specimen (with volume V_A) used in the capillary imbibition experiment (see §3.3).

A. *Multiple imbibition fronts*

The application of L-W equation to the capillary bundle configuration defined above gives for the amount of water absorbed per unit area (W_t, kg/m^2) the expression

$$W_t(t) = \frac{\rho_w}{4A} \sum_{i=1}^{N} n_i \pi d_i^2 L_i(t) \quad (7)$$

where ρ_w is the density of water at 23 °C, A is the specimen area and $L_i(t)$ is given by eq. 1 with $d=d_i$. Formally, eq. 7 is a summation (performed over the N pore size classes) of the amounts of water present in the different pores at each time t. The no-flow boundary condition derived from eq. 4 is also set in the

calculation, requiring that the capillary flow in each pore should stop once it has travelled through the entire pore length, that is, when $L_i(t) = {d_i}^{1-D_T} {L_0}^{D_T}$.

It is important to stress that this approach, adopted by Pia et al. in their modelling of capillary imbibition [8], comes out straightforwardly from choosing the said capillary bundle configuration. Indeed, in an ensemble of independent capillary tubes, the imbibition rate of each pore scales as $\sqrt{d_i}$ (eq. 1), hence the water uptake occurs with multiple imbibition fronts and the timescale of the process ends up being dominated by the largest pores.

B. *Single imbibition front*

Within a capillary bundle configuration, the only way of describing the water uptake through a single imbibition front is to define a single "average" pore diameter representing the entire microstructure. In the literature, there have been attempts to address this issue by using the average or median pore diameters obtained from MIP or other porosimetry techniques [58,62]. However, this approach showed poor agreement with experimental results, requiring the use of corrective factors to allow the fitting of eq. 1 to the experimental imbibition curves. More recently, starting from the capillary bundle configuration outlined in §2.1.1, Cai et al. calculated an 'average effective pore diameter' [40] by following a different approach. First, they expressed the imbibition rates v_{0i} (m/s) of single capillary tubes as

$$v_{0i}(t) = \frac{\alpha^3 d_i \gamma}{4\mu {\tau_i}^2} \frac{1}{h_i(t)} \tag{8}$$

which is only the non-integrated form of L-W equation, where τ_i is the tortuosity factor defined by eq. 2, $h_i(t)$ is the height reached by the liquid at time t and α is a geometrical factor (unique for all pores) representing the deviation of the pore cross-section from circularity [40], its value being equal to 1 for circular cross section and higher than 1 for other geometries [47]. Single imbibition rates v_{0i} are then weighted by the respective multiplicities n_i (eq. 6), yielding the average rate v_0

$$v_0(t) = \frac{dh(t)}{dt} = \frac{\sum_{i=1}^{N} n_i v_{0i}}{\sum_{i=1}^{N} n_i} = \frac{\alpha^3 \gamma}{4\mu h(t)} \frac{d_{ae}}{\tau_{ae}^2} \tag{9}$$

where $h(t)$ is the height reached by the single front at time t, and d_{ae} and τ_{ae} stand for 'average effective pore diameter' and 'average effective tortuosity', respectively. As shown by eq. 9, the $d_{ae}/{\tau_{ae}}^2$ ratio results from a weighted sum of the single $d_i/{\tau_i}^2$ terms occurring in eq. 8. Since small pores are numerically predominant in the microstructure of most porous materials, the value of d_{ae} obtained through this calculation turns out to be significantly smaller than the MIP-calculated average or median pore diameters. From a physical point of view, the meaning of the approach leading from eq. 8 to eq. 9 cannot be justified for a set of independent capillary tubes of different size. As discussed previously, the application of eq. 8 to such configuration would lead back to the known scenario of multiple imbibition fronts. However, based on the empirical observation that in real porous media this multiple-front dynamics tends to converge to a single front, Cai et al. made the approximation of defining an average imbibition rate as a weighted sum of the single pore rates. Albeit not formally stated, this choice may be related to the empirical evidence that capillary tubes do not have constant size over their entire length and that some connectivity exists between them, so that smaller and larger segments alternate along each tube and parallel tubes are to some extent connected to each other. Once the $d_{ae}/{\tau_{ae}}^2$ ratio has been calculated, the amount of water absorbed per unit area (W_t) is expressed by integrating eq. 9 in time, which leads to the expression

$$W_t(\mathrm{t}) = \left(\frac{\rho^2 \phi^2 {S_{wf}}^2 \alpha^3 \gamma d_{ae}}{2\mu \tau_{ae}^2} t\right)^{1/2} \tag{10}$$

When handling eq. 10, the no-flow boundary condition

$$\max[W_t] = \rho L_0 \phi S_{wf} \tag{11}$$

must be applied in order to take the height of the specimen L_0 into account.

The additional term S_{wf} in eq. 10 represents the maximum volume fraction occupied by water during the imbibition process, thus accounting for the possible incomplete saturation of the pores due to residual air. Such term is obtained by measuring the maximum amount of water absorbed by the specimens, which can be done through an immersion experiment (§3.4) as an alternative to the typical "bottom-up" imbibition test (§3.3). This fact has relevance for the practical application of the model. Indeed, since measurements by immersion have a less strict dependence on the specimen geometry, samples with a smaller size and non-regular geometry may be potentially used, limiting materials consumption and posing this modelling procedure as a sustainable alternative to the experimental laboratory measurement of sorptivity on heritage materials.

2.1.2. Pore network model

The pore network model is based on a configuration where pores are regarded as nodes connected to each other by throat channels of different size [22]. The average number of channels meeting at each node defines the connectivity of the network, expressed by a coordination number z. While nodes make up the bulk of the pore space, channels are supposed to determine the hydraulic conductivity of the system. Pore diameters obtained from MIP measurements are used to determine the size (d_i) of the different throat channels [15].

Then, by applying the Effective Medium Approximation [48], this heterogeneous network is reduced to an equivalent porous medium where throat channels are all the same size (d_{eff}) and their hydraulic conductance (g_{eff}) has the same value as in the real medium. Assuming straight cylindrical throat channels of length y [15], the individual hydraulic conductances g_i and the effective conductance g_{eff} can be calculated through the formula

$$g_x = \frac{\pi}{128}\frac{d_x^4}{y} \tag{12}$$

where the subscript x stands for "i" or "eff".

The effective diameter d_{eff} in the equivalent medium (also termed hydraulic diameter) is obtained by requiring that the incremental pressure changes induced when the individual conductances g_i are replaced by g_{eff} should average to zero. That is tantamount to saying that both the real and the equivalent medium should experience the same net flow if subjected to the same boundary conditions. This self-consistency requirement is represented by the equation [48]

$$\sum_{i=1}^{N} \frac{g_{eff}-g_i}{g_i+\left(\frac{z}{2}-1\right)g_{eff}} = 0 \tag{13}$$

where N is the number of pore size classes (provided by MIP) and z is the average coordination number characterizing the topology of the pore space, whose values can range from 2 up to infinity. When z=2, the channels are arranged in series and the conductivity reaches its lowest possible value. On the other hand, as the coordination number tends to infinity, the channels progressively switch to a parallel arrangement, and the conductivity reaches its maximum value. Eq. 13 can be solved for different values of z, yielding an effective conductance g_{eff} and a corresponding pore diameter d_{eff} for each z value.

Within the equivalent pore space defined by d_{eff}, the capillary uptake can be described through the modified form of L-W equation

$$W_t(\mathrm{t}) = \left(\frac{\rho^2\phi^2{S_{wf}}^2\delta d_{eff}\gamma}{4\mu\tau_{av}}t\right)^{1/2} \tag{14}$$

where δ is a pore shape factor accounting for the deviation from circularity of the cross section of d_{eff}. More specifically, this factor is defined as the ratio between d_{eff} and the hydraulic diameter of the smallest pore with circular cross section that can be circumscribed to it [15,49]: accordingly, its values can range between 1 and 0 (δ=1 for a perfectly circular pore and δ<1 for other geometries). Together with the no-flow boundary condition represented by eq. 11, eq. 14 describes a single-front imbibition process. As only difference from Benavente's formula, the maximum saturation S_{wf} (eq. 21) is introduced and the average tortuosity τ_{av} is calculated according to Comiti and Renaud's equation (eq. 3).

2.2. Modelling of protective performance

A mechanistic model of pore hydrophobization was proposed to describe the effect of protective treatments on capillary imbibition. This model was conceived starting from already established evidence about the behaviour of silicon-based treatments [9] and experimental observations here reported concerning the specific interaction between the treatments and stones under study. There is a long-standing literature attesting that silane and siloxane-based treatments behave as non-filming agents [6,9]. This means that their protective effect is not achieved through the formation of a continuous surface film but relies on the ability to penetrate up to some mm under the stone surface, settling on the pore walls and producing nm-thick deposits, which are able to protect pores from water ingress without occluding them.

Some of the observations made on treated stone specimens during this research confirmed the above statements and provided the basis for the main assumptions of the model.

First, MIP analysis conducted on cubic samples that had been treated on all six faces indicated that the application of the treatments did not result in either a visible reduction in the stone porosity or a significant modification of its pore size distribution, thus suggesting that the majority of the pores had not been occluded. Moreover, as far as it was possible to assess through the SEM technique, the treatments did not alter the stone surface morphology by concealing grain boundaries and clogging pore apertures, while vapour permeability measurements did not detect a significant reduction in the stone vapour diffusivity (indeed, this reduction was always less than 40%). At the same time, static contact angles on treated surfaces were steadily higher than 120 °C, hence the latter displayed a high degree of water repellency, indicating that the treatments produced a widespread, if very thin, coverage of the outermost pore surface.

One further crucial observation, based on the testing of several different treatments, was that low-molecular-weight compounds are apt to impart a greater and more persistent hydrophobizing effect. By suggesting that the size of product components may be a discriminating factor for the protective performance, this led to the general hypothesis that small-size treatments are more effective because they are able to penetrate into a wider range of pores or, seen from another perspective, the larger are the pores, the easier they allow the penetration of the treatments. Based on this hypothesis, two assumptions were made in the modelling of the stone-coating interaction.

The first assumption is that large pores tend to be protected better than small pores owing to the fact that they allow for an easier penetration of the treatments. Besides that, having a lower specific surface area, they also require a lower amount of treatment at corresponding pore volume to achieve a complete surface coverage. According to this assumption, a greater number of pores with a large diameter are hydrophobized with respect to smaller pores (Figure 1c). Treatments comprising nanoscale aggregates (§3.5) should also behave according to this principle: indeed, the larger are the aggregates, the lower should be their probability of entering small pores. The second assumption is that hydrophobized pores reduce the rate of water absorption to an extent depending on the penetration of the treatments.

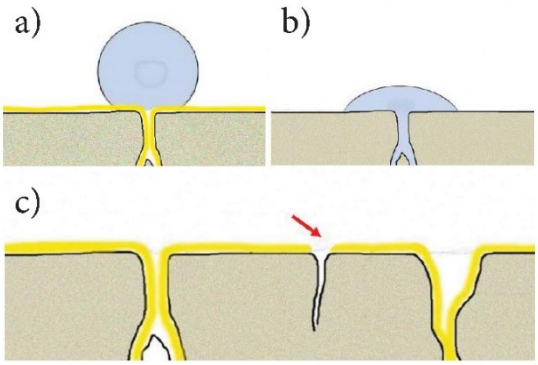

Figure 1. **Assumptions made for the modelling of pore hydrophobization: (a-b) hydrophobized pores reduce the rate of water absorption to an extent depending on the penetration of the treatments; (c) a greater number of large pores are hydrophobized compared to smaller pores (see arrow).**

According to the first assumption, it was expected that the water absorption rate $(v_i)_t$ of each pore with diameter d_i after the application of the treatments should be correlated to its respective value in the untreated stone $(v_i)_{nt}$ (eq. 6) through some function $f(d_i)$, with the obvious condition that $f(d_i) \leq 1$ for any value *of* d_i. From a physical point of view, $f(d_i)$ is a damping factor that accounts for the effect of protective treatments on the capillary uptake.

In the framework of Cai's model, this factor was introduced into the equation for the water absorption rate (eq. 9), leading to the expression for the amount of water absorbed per unit area (W_t)

$$W_t(\mathrm{t}) = \left(\frac{\rho^2 \phi^2 {S_{wf}}^2 \alpha^3 \gamma}{2\mu} \frac{\sum_{i=1}^{N} n_i f(d_i) \frac{d_i}{\tau_i^2}}{\sum_{i=1}^{N} n_i} t \right)^{1/2} \qquad (15)$$

Upon testing different one-parameter functions and fitting the corresponding forms of eq. 15 to the absorption curves of treated stones (all other parameters being kept constant), it was found that the exponential

$$f(d_i) = e^{-\left(d_i / d_0\right)} \qquad (16)$$

was best suited to represent the water absorption reduction. Then, the parameter d_0 was obtained through univariate regression.

Regarding Benavente's model, a similar approach was adopted to modify eq. 14. In this latter case, an exponential law analogous to eq. 16 was applied to the hydraulic conductivity g_i (eq. 12), leading to the modified expression

$$(g_i)_t = \frac{\pi}{128} \frac{d_i^4}{y} e^{-\left(d_i / d_0\right)} \qquad (17)$$

Then, by solving eq. 13 with the modified conductivity $(g_i)_t$, a new value of the effective diameter d_{eff} was calculated, the new effective diameter being now a function of d_0. Finally, the value of d_0 was obtained by fitting the modified form of eq. 14

$$W_t(\mathrm{t}) = \left(\frac{\rho^2 \phi^2 {S_{wf}}^2 \delta d_{eff}(d_0) \gamma}{4\mu \tau_{av}} t \right)^{1/2} \qquad (18)$$

to the experimental absorption curve of the treated stone.

3. **Materials and methods**

3.1. Stone materials

Four sedimentary rocks, characterized by different petrophysical and petrological properties [50], have been selected for this study. Lumaquela de Ajarte (from Treviño, Castile and León, Spain) is a biomicrite with creamy greyish colour, composed of shell fragments in a carbonate matrix consisting of recrystallized fossils (>99% calcite). Balegem stone (from Balegem, East Flanders, Belgium) is a fossil-rich siliceous clastic arenite (grain size of 0.1-0.2 mm with, occasionally, up to 7 mm large particles) of light greyish colour, composed of quartz (~40%), feldspars (~5%) and foraminifera set in a sparite cement (~55% calcite). Obernkirchen stone (from Bückeberge, Lower Saxony, Germany) is a fine to medium-grained (0.04-0.1 mm), well-sorted, porous quartz-arenite with colour ranging from white-grey to light orange. It is mainly composed of quartz grains (98%), along with small amounts of feldspars, dolomite and opaque minerals; the grain-supported texture is characterised by a kaolinite authigenic matrix, growing on grain surfaces, partly filling pores and forming bridges together with dolomite. Schlaitdorf stone (from Schlaitdorf, Baden-Württemberg, Germany) is a whitish to yellowish coarse-grained quartz-arenite (grain size of about 1 mm), characterized by well-sorted quartz grains (~70%) and, subordinately, altered feldspars (~3%). This clastic fraction is dispersed in a matrix consisting of dolomite (~9%), kaolinite (~11%) and small amounts of illite.

3.2. Mercury Intrusion Porosimetry

Mercury Intrusion Porosimetry (MIP) measurements were performed on two specimens per stone (ca. 0.5 cm^3 in size) in the range from 150-0.001 μm, using a Pascal 140 Mercury Porosimeter (Thermo Fischer) equipped with a high pressure module to extend the porosity range of investigation, in compliance to the ISO standard 15901-1 [51].

3.3. Determination of water absorption by capillarity

Water absorption by capillarity was measured for 96 h on 30 specimens (5×5×2 cm^3 prisms) per stone according to the European standard EN 15801 [7]. The direction of the flow was along the shortest axis, hence the specimen height (L_0) and its cross-sectional area (A) were 2 cm and 25 cm^2, respectively.

All of the selected stones did not show any visible orientation of sedimentary planes, either by naked-eye or microscopy observation, hence a possible effect of material anisotropy relative to the sedimentary planes was ruled out and absorption measurements were performed along the privileged direction defined in the preparation of the specimens. This does not exclude the possibility that other anisotropy features, such as the crystallographic preferred orientation of mineral grains, may be present, although their impact on the directional dependence of sorptivity should be less significant. Of the four stones considered in the study, only Obernkirchen has been the subject of a considerable number of scientific publications. For this stone, an anisotropy of 9% was reported among the values of sorptivity in the X and Z directions [4], which is much lower than seen on other stones displaying a well visible orientation of sedimentary planes, where values of up to 70% have been observed [34]. Furthermore, as it will be appreciated (§4.1), this supposed anisotropy is smaller than the standard deviation of sorptivity measurements.

Prior to the test, the specimens were immersed in deionized water for 1 h in order to remove any excess soluble salts, dried in oven at 65 °C until constant weight and stored in a silica gel desiccator for another 24 h. Then, they were placed on water-soaked filter paper pads (Ahlstrom-Munktell laboratory filter paper, 1288 grade) and the absorption of water was monitored gravimetrically. To avoid the superposition of any evaporation process, the test was conducted in closed vessels.

At increasing time intervals (0, 10 min, 20 min, 30 min, 60 min, 4 h, 6 h, 24 h, 48 h, 72 h and 96 h), each specimen was blotted with wet deerskin to remove water drops adhering to the surface, then quickly weighed and returned to the vessel as soon as possible (about 15 seconds). The amount of water absorbed per unit area as a function of time (W_t, mg/cm^2) was calculated through the formula

$$W_t(t) = \frac{m_s(t) - m_d}{A} \qquad (19)$$

where m_S(t) is the weight of the specimen at time t, m_d is its dry weight (at t=0) and A is the cross-sectional area (25 cm^2). The results were plotted as W_t vs. $\sqrt{t}$. In order to quantify capillary imbibition kinetics, the slope of the curve during the first stage of the absorption, i.e., the water absorption coefficient or sorptivity (C, mg·cm^{-2}·$s^{-1/2}$), was calculated by linear fitting of the first points of the curve, while W_t values at 96 hours (W_f) were used to describe the hydric behaviour in the subsequent regime. The choice of this particular time was conventional and due to the organizational requirements of laboratory work, according to which each set of measurements could not be scheduled for more than 5 days. The weight increase of stone specimens at 96 hours was about 2%, that is, very close to the threshold value prescribed by the European standard (1%), so it was considered suitable to represent a quasi-stationary condition.

3.4. Determination of maximum water saturation

Water absorption by immersion was measured on 20 specimens (5×5×5 cm^3 cubes) per stone following the European standard EN 13755 [52].

This experiment yields the 'effective' porosity (P, vol%), which is the actual porosity accessible to water during imbibition, determined as

$$P = \frac{\rho_g}{\rho_w} \cdot \frac{m_s - m_d}{m_d} \cdot 100 \qquad (20)$$

where ρ_g is the bulk density of the stone, ρ_w is the density of water at 23 °C, m_d and m_s are the masses of dry (d) and saturated (s) stone specimens, reported by Lezzerini et al. [50].

From P, the maximum water saturation relative to the MIP porosity (S_{wf}, expressed as volume fraction) was obtained as

$$S_{wf} = \frac{P}{\phi} \qquad (21)$$

where ϕ is the MIP open porosity.

3.5. Protective treatments

Two nanocomposite formulations (Table 1) based on alkylalkoxysilane reactive sols and TiO_2 nanoparticles were applied onto the four stones for 6 h by capillary absorption. These products have been thoroughly characterized in previous articles [53,54]. Briefly, ANC consists of silane monomers (40% w/w) and TiO_2 nanoparticles (0.12% w/w) in 2-propanol, while WNC is based on silane oligomers (15% w/w) and TiO_2 nanoparticles (0.96% w/w) in water. Upon hydrolysis and condensation of the silane units, the sols give rise to organosilica gel networks, which impart water-repellent features to the treated stones, while the presence of TiO_2 NPs is expected to add photocatalytic and self-cleaning properties.

Water absorption measurements on treated stone specimens were performed several months after the application of the treatments, so as to eliminate or minimize any bias on the protective performance that might be related to the different kinetics of gelification and curing of the two products. The protective effectiveness was quantified through the relative sorptivity (C_t/C_{nt}), which is the ratio of sorptivity values measured on each specimen before (nt) and after (t) the application of the treatments.

The possible role of the nanoscale size of product components in their interaction with stones has been discussed in §2.2. According to the proposed model of pore hydrophobization, nanosized aggregates should better protect pores with increasing diameter, because the latter allow them to penetrate more easily. Regarding the individual role of titania nanoparticles in the interaction, it is important to specify that in one previous paper [54] the protective performance of WNC/ANC was compared with those of the respective TiO_2-free silane matrices and virtually no difference was observed in their ability to reduce capillary absorption. This appears justified at the light of what is known about the composition of the products. Indeed, by analysing the particle size of the liquid dispersions, it was seen that the matrix of WNC, consisting of silane oligomers, is itself made up of supramolecular aggregates with a diameter of about 80 nm [54]. Moreover, titania nanoparticles were shown to interact with the matrix, probably forming aggregates that explain the particle size of 106 nm measured in the composite (Table 1) [54]. In the case of ANC, the matrix has molecular-size components (i.e., below the nanoscale), yet titania nanoparticles are quite small in size (25 nm) and their concentration is too low to have any detectable effect on the stone-coating interaction.

Table 1. Main properties of the selected water-repellent products: composition, solvent, particle size (nm) and viscosity (mPa·s).

Product	Composition	Solvent	Particle size	Viscosity
WNC	alkylalkoxysilane oligomers (15% w/w) and TiO_2 nanoparticles (0.96% w/w)	water	106	10
ANC	alkylalkoxysilane monomers (40% w/w) and TiO_2 nanoparticles (0.12% w/w)	2-propanol	25	7

4. **Results and discussion**

4.1. Characterization of stones

Microstructural analysis performed by MIP shows that the selected stones can be classified as medium-high to medium-low porosity materials (Table 2): at the top end, Ajarte and Obernkirchen show very similar medium-high values of open porosity (~24%), and, at the bottom end, Balegem has a medium-low value (9.9%), while Schlaitdorf lies in the middle (16%). At the same time, median pore diameters (Table 2) and pore-size distributions (Table 2 and Figure S1) indicate that most of the pore volume of Ajarte and Balegem concentrates in the range below 10 μm, while Obernkirchen and Schlaitdorf display a significant amount of pores larger than 10 μm and the latter stone has, among all, the highest relative abundance of pores in the uppermost size interval (>50 μm).

Table 2. Mean values of open porosity (ϕ, vol%), average pore diameter (d_{av}, μm), median pore diameter (d_m, μm), bulk density (ρ_g, g/cm^3) and pore-size distribution (expressed as ϕ% of four size classes: P1 >50 μm; P2 50-10 μm; P3 10-1; P4 <1 μm) of the selected stones. Standard deviations are shown in brackets.

Name	ϕ	d_{av}	d_m	ρ_g	P1	P2	P3	P4

Ajarte	23.5 (0.4)	0.17 (0.03)	1.96 (0.04)	2.08 (0.01)	3.9 (0.9)	15 (3)	47 (3)	33 (2)
Balegem	9.9 (0.8)	0.28 (0.06)	1.2 (0.3)	2.50 (0.03)	4 (1)	10 (1)	39 (6)	46 (7)
Obernkirchen	24.1 (0.1)	0.8 (0.3)	11.1 (0.6)	2.08 (0.06)	5.7 (0.6)	47 (2)	35.7 (0.3)	12 (1)
Schlaitdorf	16 (1)	0.38 (0.04)	8 (4)	2.23 (0.02)	8 (2)	33 (8)	38 (7)	20 (3)

In general terms, the kinetics of capillary imbibition shows two well distinct regimes: first, the water uptake is linear with $\sqrt{t}$, whilst its rate is drastically reduced in the subsequent stage of the process: the first stage corresponds to the saturation of the free accessible porosity by the genuine capillary imbibition mechanism, whereas the second one coincides with a diffusion process where trapped air bubbles slowly dissolve into water allowing the saturation of the smallest pores [15]. The absorption coefficient or sorptivity (C, §3.3) represents the kinetics of the early capillary-driven imbibition, while the amount of water absorbed at 96 h (W_f, §3.3) and the maximum saturation measured by immersion (S_{wf}, §3.4) refer to the second diffusional stage.

Sorptivity values in Table 3 show that the four stones have distinct, though not overly different, imbibition rates, whose relationship to the main microstructural parameters is however not entirely consistent. This stands out clearly from a comparison with Table 2: whilst the volume fraction of large pores (>10 μm), i.e., (P1+P2)·ϕ, being larger in Schlaitdorf (6.7%) with respect to Ajarte (4.5%) and Balegem (1.4%), explains the trend of sorptivity values in these three stones (5.3 as compared to 4.5 and 1.7 mg·cm^{-2}·s$^{-1/2}$, respectively), the same correlation does not hold for Obernkirchen, which shows by far the highest fraction of large pores (12.6%) but not a commensurately high sorptivity (3.3 mg·cm^{-2}·s$^{-1/2}$).

Other relevant information is provided by S_{wf} values (Table 3). These values point out that, with the notable exception of Ajarte (0.89), stones are far from reaching a complete saturation of the pore space. Balegem and Schlaitdorf are indeed saturated up to about 70% of the total pore volume measured by MIP, while Obernkirchen remains below 60%, in fairly good agreement with literature data, which report for this stone an open porosity ranging between 18.6% [34] and 21% [55] but just 10% 'effective', i.e., water-accessible, porosity [22]. This can be explained by the fact that capillary imbibition at atmospheric pressure is limited by the air diffusion kinetics, whereas air is completely removed from samples prior to the MIP measurement. How large is the fraction of water-accessible pores probably depends on the geometry and connectivity of the pore space in each stone.

By inspecting the trend of imbibition curves in Figure 2, which duly consist of a $t^{1/2}$–linear section (the one serving as base for the calculation of sorptivity) followed by a more or less flat section (also called plateau region), it can be noticed that most of the pores are filled during the early stage of the imbibition process. However, the non-completely flat profile of some of the curves indicates that a residual fraction of the pores continue to absorb water even after the early imbibition stage has come to an end, because the co-presence of air and, in general, differences in capillary pressure across the medium are likely to delay the filling of the smallest pores. In particular, residual pores give a non-negligible contribution to the overall capillary uptake in the case of Ajarte, as the steeper profile of the later section of the curve indicates.

One last consideration can be made by comparing W_f and S_{wf} values in Table 3. If these values are converted to the same measuring units (mg/cm^2), it turns out that the amount of water absorbed by immersion (W*) is always lower than the amount absorbed at the end of the capillary imbibition experiment (W_f) and much closer to the value absorbed during the first $t^{1/2}$- like stage of the process, to which L-W equation refers. Therefore, using S_{wf} to represent the upper bound saturation of specimens in the modelling of capillary flow (§2.1.1.A) can be regarded as an acceptable approximation.

Table 3. Sorptivity (C, mg·cm^{-2}·s$^{-1/2}$), amount of water absorbed per unit area at 96 h (W_f, mg/cm^2), maximum water saturation (S_{wf}), effective porosity (P, vol%) and corresponding amount of water absorbed per unit area (W*) for the selected stones. Standard deviations are reported in brackets.

	C	W_f	P	S_{wf}	W*
Ajarte	4.5 (1.0)	434 (22)	20.7	0.89	414
Balegem	1.7 (1.1)	146 (52)	6.3	0.59	124
Obernkirchen	3.3 (0.7)	254 (18)	10.1	0.42	202

Schlaitdorf	5.3 (1.5)	223 (20)	10.0	0.65	200

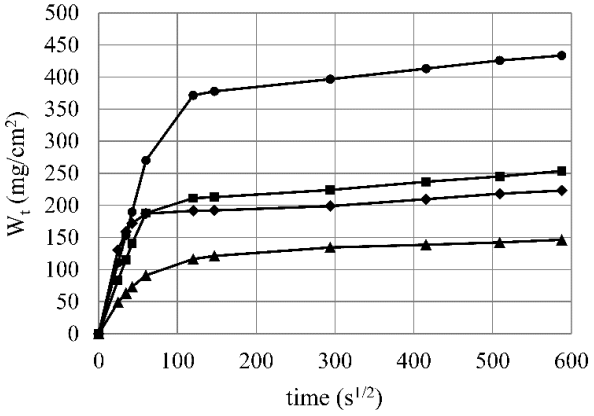

Figure 2. Capillary water absorption curves of the selected stones: Ajarte (●), Balegem (▲), Obernkirchen (■), Schlaitdorf (◆).

4.2. Modelling of capillary imbibition

Upon applying L-W equation (eq. 1) to predict the kinetics of capillary imbibition, two possibilities were taken into account. Imbibition may either proceed with multiple fronts (i.e., one separate front for each of the pore classes that make up the porous microstructure) or be characterized by a homogeneous, piston-like behaviour. The latter was verified experimentally by X-ray CT measurements on materials with a well-sorted grain structure such as diatomite [56] and Berea sandstone [57]. As discussed in §4.1, this pattern does not perfectly apply to the absorption behaviour of many natural stones, because some fraction of the pores are filled more slowly than the others. However, taken as an approximation, the single-front hypothesis still represents an acceptable description of reality while bringing considerable simplification in the modelling of the imbibition process models based on L-W equation usually rely on it (with few exceptions [8]).

4.2.1. Capillary bundle model

A. *Multiple imbibition fronts*

Within the capillary bundle model explained in §2.1.1, the hypothesis of multiple imbibition fronts (§2.1.1.A) was initially evaluated. The application of eq. 7 resulted in a substantial overestimation of the imbibition rate, as shown in Figure S2. In particular, data analysis clarified that, for all pores but those below 0.01 μm, the meniscus velocity predicted by the model is faster than the average experimental one. The only possibility of making the simulated curve reproduce the experimental trend is to choose contact angle values in the range 89°-90°, which are physically unreasonable. Besides that, no contact angle calibration would be feasible in this range due to the rapid changing of the cosine function in the vicinity of 90°.

B. *Single imbibition front*

In order to set the restraint of a single imbibition front within a capillary bundle configuration (§2.1.1.B), Cai et al. [40] proposed weighting the imbibition rates of single pore classes by their respective multiplicity (see eq. 9). Since small pores are numerically predominant in the stone microstructure, this weighted sum yields an average imbibition rate that is lower than most single-pore rates, thus correcting the overestimation made under the multiple-front hypothesis. Cai's formula (eq. 10) also includes an experimental term (S_{wf}) accounting for the incomplete water saturation of the pores and a geometrical factor (α) accounting for their non-circularity (§2.1.2). This factor can be determined through a calibration procedure.

As regards the first part of the absorption curves (approximately up to 1 hour), Cai's model is able to describe the imbibition process fairly accurately (Figure 3). Furthermore, the range of calibrated α values (Table 4) turns out to be in good agreement with what is reported by Cai et al. [40]. On the other hand, the model is not able to describe the water uptake occurring in the so-called diffusional stage (Figure 3). Indeed, according to the single-front assumption, all pores are supposed to follow the same imbibition dynamics until the stone attains its maximum saturation S_{wf}. From then, no further increase in weight is permitted and the curve profile should become flat. As discussed in §4.1, none of the absorption curves of the four stones ends up with a completely flat profile, because some of the pores are filled later than others. Therefore, the model properly only accounts for the first stage of the imbibition process. At the same time, it can be observed from

a practical viewpoint that using the maximum saturation parameter S_{wf} (Table 3) does not lead to exceedingly great errors in the approximation of the curve endpoint.

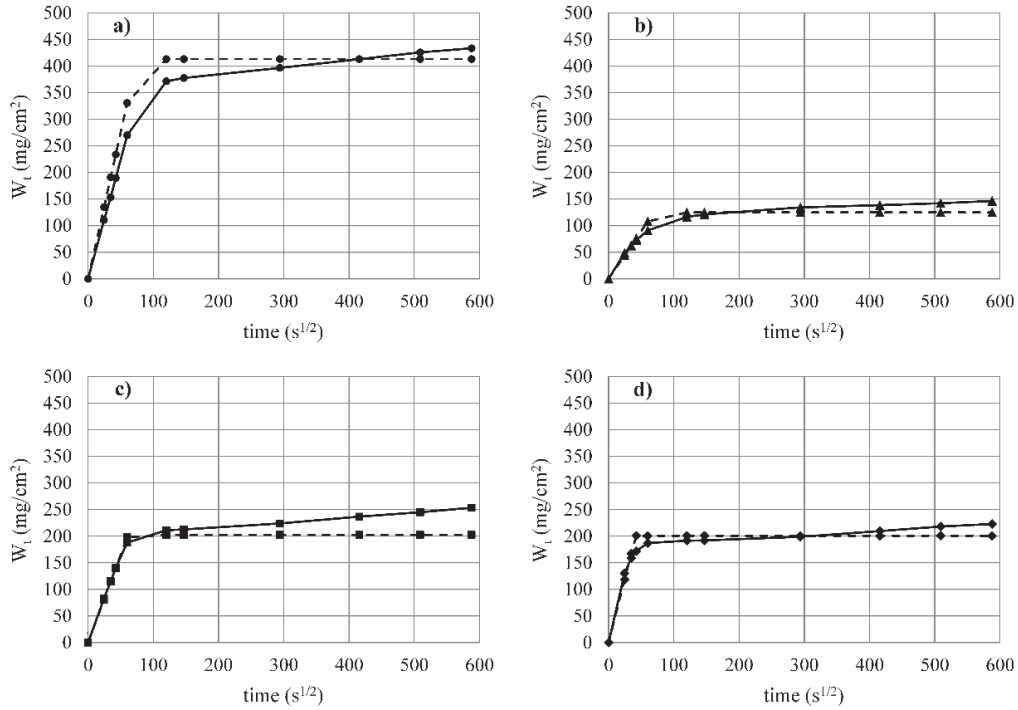

Figure 3. Comparison of experimental absorption curves (full line) and curves simulated through eq. 10 with calibrated values of *α* (dashed line) for: a) Ajarte; b) Balegem; c) Obernkirchen; d) Schlaitdorf.

The need of calibrating the geometrical factor *α* limits the possibility of using the model as a predictive tool for the determination of sorptivity. However, a glance at Table 4, where calibrated α values are compared with the volume fraction of large pores obtained by MIP (P1, d>50 μm), suggests that stones with P1<6% display α values very close to 1. Furthermore, the moderate variability of this geometrical factor does not have a significant effect on the calculation of sorptivity. Therefore, it may become possible to skip the calibration step by adopting a heuristic approach, assigning α=1 for all substrates with P1<6%. This allows to determine sorptivity with acceptable approximation, as a comparison between experimental (C_{exp}) and calculated (C_{calc}) values reveals (Table 4), hence the model seems fit for the purpose of being used as a predictive tool in the case of stones with P1<6%. On the other hand, for stones with a greater P1 fraction, such as Schlaitdorf (8.4%), whose calibrated α value is considerably higher (1.5), such a simple approach cannot be applied. Further tests involving additional substrates with different microstructure and total open porosity would be necessary in order to evaluate the relationship between α and the P1 fraction.

Table 4. Experimental values of sorptivity (C_{exp}, mg·cm^{-2}·s$^{-1/2}$); values of sorptivity (C_{calc}) predicted by eq. 10 with non-calibrated values of *α*, that is, 1 for Ajarte, Balegem, Obernkirchen and 1.5 for Schlaitdorf; calibrated values of α; volume fraction of large pores (>50 μm, P1, vol%). Standard deviations are shown in brackets.

	C_{exp}	C_{calc}	α	P1
Ajarte	4.5 (1.0)	5.5	1.0	3.9
Balegem	1.7 (1.1)	1.7	1.0	4.1
Obernkirchen	3.3 (0.7)	3.3	1.1	5.7
Schlaitdorf	5.3 (1.5)	4.9	1.5	8.4

4.2.2. Pore network model

An alternative approach to the modelling of capillary imbibition can be pursued by adopting a pore network configuration (§2.1.2). According to this approach, pores are no longer regarded as parallel tubes,

but rather as a network of nodes connected by throat channels. Following the procedure illustrated in §2.1.2, if an assumption is made on the pore connectivity of this network, then its hydraulic conductivity can be described in terms of an equivalent medium with an effective diameter d_{eff}. To the best of our knowledge, Benavente et al. were the first to apply this procedure to the study of capillary imbibition in natural stones [15], introducing a modified form of L-W equation (eq. 14).

In the present study, Benavente's model was applied to the four selected stones, after introducing the S_{wf} term in eq. 14 to account for the incomplete saturation of the specimens. Moreover, the pore shape factor δ and the coordination number z (on which the effective diameter d_{eff} depends) were determined through a calibration procedure.

Regarding the potentiality of the model, it can be observed that the first stage of the imbibition process is accurately described. Indeed, a very close match is found between the experimental and calculated values of sorptivity, as it appears from the nearly perfect superposition of the curves (Figure 4). On the other hand, as discussed for Cai's model (§4.2.1.B), only a rough approximation of the diffusional stage can be given, since the model cannot account for the possible filling of residual pores after the primary imbibition front.

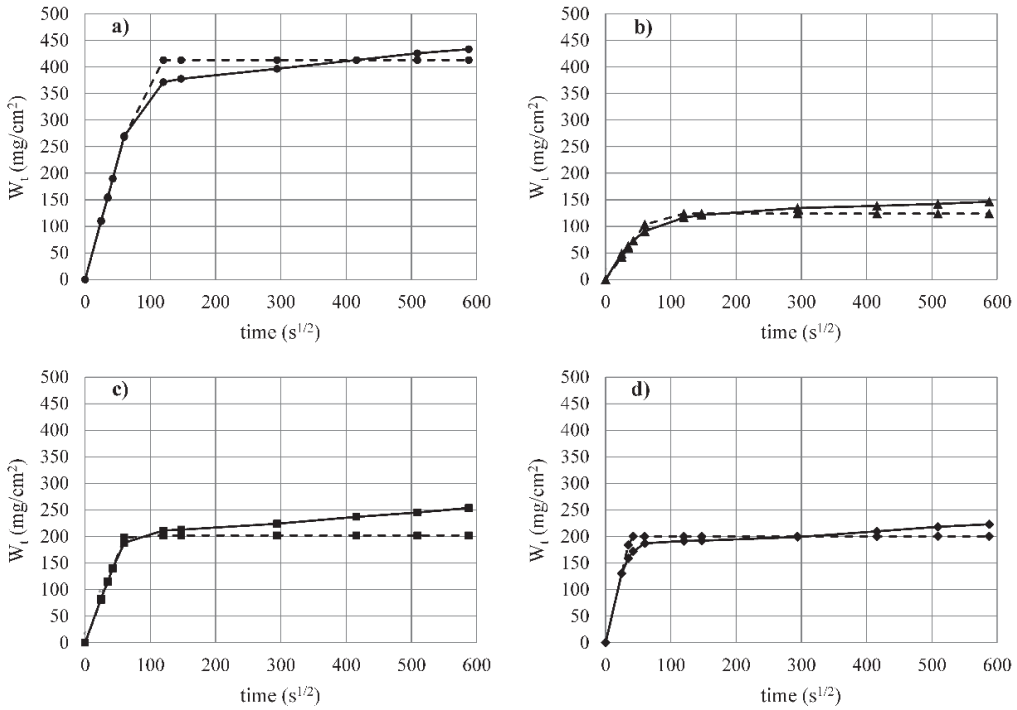

Figure 4. Comparison of experimental absorption curves (full line) and curves simulated through eq. 14 with calibrated values of δ and z (dashed line) for: a) Ajarte; b) Balegem; c) Obernkirchen; d) Schlaitdorf.

The calibration of the pore shape factor δ in eq. 14 yielded values between 0.7 and 1 (Table 5). As for the coordination number z, the value of 2 was seen to fit very well to Ajarte, Balegem and Obernkirchen, while a value of 2.3 was obtained for Schlaitdorf (Table 5). These values are found to be in good agreement with those of other stone substrates reported by Benavente, being in all cases close to 2.

Table 5. Experimental values of sorptivity (C_{exp}, mg·cm^{-2}·s$^{-1/2}$); values of sorptivity (C_{calc}) predicted by eq. 14 with δ=1, z=2 for Ajarte, Balegem, Obernkirchen and δ=1, z=2.3 for Schlaitdorf; calibrated values of the coordination number (z) and pore shape factor (δ); values of the effective diameter (d_{eff}, µm) obtained from calibrated z.

	C_{exp}	C_{calc}	z	δ	d_{eff}	P1
Ajarte	4.5 (1.0)	5.1	2.0	0.78	0.006	3.9
Balegem	1.7 (1.1)	2.0	2.0	0.74	0.014	4.1
Obernkirchen	3.3 (0.7)	3.7	2.0	0.81	0.014	5.7
Schlaitdorf	5.3 (1.5)	5.1	2.3	0.99	0.033	8.4

As a next step, it is worth considering whether the model can (under some approximations) be used in a predictive way with still acceptable accuracy. First, δ is approximated to 1 for all stones. Regarding the coordination number z, the same heuristic criterion can be applied as for the choice of α values in eq. 10 (§4.2.1.A) and a value of z=2 is assumed for stones with a P1 fraction lower than 6%. Under these approximations, the model seems capable of working as a predictive tool, as the approximated values of sorptivity (C_{calc}) match quite well with the experimental ones (Table 5). On the other hand, on stones with a higher z value and a greater P1 fraction, among which is Schlaitdorf, further investigations should be performed in order to assess whether the value of z=2.3 can be generalized to a class of materials with a significant fraction of large pores.

One final remark is appropriate concerning the implication of having z values close to 2, which is the lowest possible value of pore connectivity (§2.1.2). This allows to estimate sorptivity with considerable accuracy, but also postulates values of 'effective' pore diameter (d_{eff}, Table 5) that are one to three orders of magnitude lower than the MIP average and median pore diameters, respectively (Table 2). At the same time, if the latter are used to represent the average capillary size in L-W equation, the result is a significant overestimation of sorptivity, as also reported by Raimondo et al. [58], hence these parameters cannot be relied upon to predict the imbibition rate. From the above premises, a possible explanation of this fact may be that MIP average parameters completely overlook the way that pores are arranged within the stone microstructure, i.e., their connectivity. Indeed, z=2 means that the flow dynamics occurs in a series arrangement of pores, where the smallest pores substantially control the overall process. This is consistent with evidence coming from experimental research and with theoretical models of capillary imbibition in soil science, where it is found that imbibition starts from the smallest pores, which exert the highest capillary pressure. Moreover, the limit condition of a series arrangement of pores involves that the capillary flow occurs in a 1D geometry, in agreement with the initial hypothesis of a single imbibition front (§4.2).

4.2.3. Comparison of the two models

Starting from the same experimental information and relying on very simple computational tools, both Cai's and Benavente's models showed the ability to provide a fairly accurate description of the first stage of the imbibition process. A common feature of these models is that they describe the capillary uptake in terms of a single imbibition front, thus going beyond the most rudimentary description of the pore space as an ensemble of independent capillary tubes. Cai's model achieves this by adopting an essentially heuristic approach (§2.1.1.B) that involves less parameters to be dealt with, whilst Benavente's model implies a more elaborated hypothesis on the connectivity of the pores and provides greater insight into the relationship between stone microstructure and flow dynamics (§2.1.2).

Both models also showed the potential to be used as predictive tools for the estimation of sorptivity in a circumscribed number of cases, which depend on the stone microstructural characteristics and, specifically, the presence of a small enough (<6%) fraction of large pores. When this condition is fulfilled, these models are easily implementable and promising methodologies with possible application to the study of heritage porous materials. Indeed, even though other modelling approaches, based on continuum mechanics, would be able to yield much more accurate results, also allowing to extend the description of the capillary uptake to longer timeframes, these approaches require advanced numerical analysis tools and, to be properly run, non-trivial experimental information. Therefore, for the kind of application envisaged in this study, their implementation may fail to meet the requirements set by the heritage field in terms of limited sampling and, not least, simplicity of use.

4.3. Modelling of protective performance

The potentiality of both models was also assessed in simulating the reduction of water absorption after the application of protective treatments. To this end, a very simple mechanistic model (§2.2) was devised to represent the effect of the treatments on the permeability of the pores to liquid water and, combined with the two models of capillary imbibition, the decrease in the water absorption rate. Two silicon-based treatments including small amounts of TiO_2 nanoparticles (§3.5) were chosen to validate the mechanistic model. It is worth remembering that these treatments have markedly different properties: one (WNC) is basically a dispersion of silane oligomers and TiO_2 nanoparticles in water, while the other (ANC) consists of alcohol-based silane monomers with a small loading of TiO_2 nanoparticles. The different aggregation state (oligomers/monomers) and size of these products' components (nearly 100 nm for silane oligomers, below the nanoscale for monomers) are apt to represent a test bed for the fundamental model assumption that small

pores are more difficult to protect as compared to larger ones and thus protective treatments having bulkier components tend to be less effective than those with smaller-sized ones.

As it can be observed in Figure 5, where the relative sorptivity (C_t/C_{nt}, §3.5) of WNC/ANC is plotted against the fraction of pores below 1 μm in the microstructure of the four untreated stones (P4, Table 2), both products achieve a high degree of protective effectiveness: C_t/C_{nt} values range between 0.02 and 0.04, which indicates a reduction in the capillary uptake by as much as 96-98%. However, what is more interesting, the protective performance of the treatments improves as the fraction of small pores is decreased. The stone with the lowest P4 fraction, Obernkirchen, shows indeed the highest reduction in the capillary uptake and the reverse can be said about Balegem. Two distinct trends among the products can also be noticed, for not only is the protective effectiveness of WNC steadily lower with respect to ANC but it also has a more visible dependence on the stone microstructure. The correlation between the protective effectiveness and the fraction of small pores (not the total open porosity) confirms that this class of pores plays a critical role in the stone hydrophobization. Moreover, the different behaviour of the treatments finds a logical explanation in their different penetration ability with regard to small pores: indeed, the bulkier macromolecular components of WNC are probably more impeded when it comes to protect pores with submicrometric diameter, whereas the molecular-size components of ANC are more likely to freely enter and protect most of the pores, so the performance of this product in terms of water absorption reduction is less influenced by the stone microstructural features.

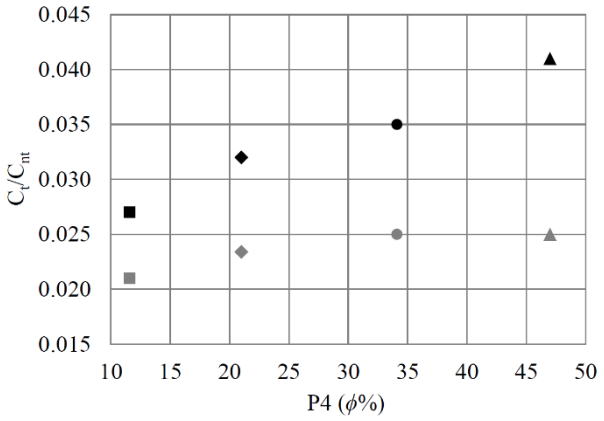

Figure 5. Correlation between the volume fraction (over total open porosity) of pores with diameter lower than 1 μm (P4, Table 2) in untreated stones and the relative sorptivity (C_t/C_{nt}) of specimens of Ajarte (●), Balegem (▲), Obernkirchen (■) and Schlaitdorf (◆) stones treated with WNC (black) and ANC (grey).

The proposed mechanistic hypothesis of pore hydrophobization led to introduce an additional parameter d_0 into Cai's and Benavente's models (§2.2). The modified equations of capillary flow (eqs. 15 and 18) were fitted to the experimental absorption curves of treated stones and the value of d_0 was determined by univariate regression. The results obtained through this approach will only be given here in connection with Cai's model, due to its greater ease of handling (see §4.2.3), but an analogous procedure can also be adopted for Benavente's.

The absorption curves of specimens treated with WNC and ANC were correctly simulated by eq. 15 (Figure 6). As most of these curves (Ajarte making the only exception) have a quasi-linear profile, showing no plateau region during the first 96 hours, the simulation was able to account for the whole absorption dynamics. Therefore, as it can be observed in Table 6, there is a good agreement between calculated and experimental values of both sorptivity (C_t) and amount of water absorbed at 96 h (W_f).

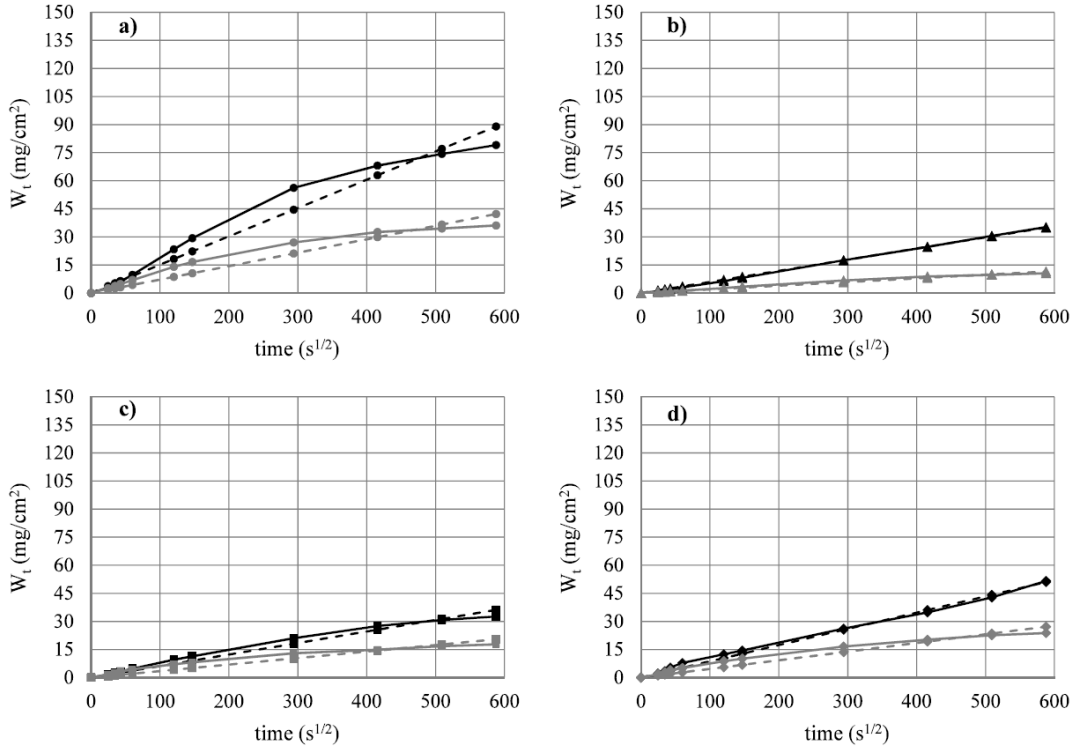

Figure 6. Comparison of experimental absorption curves (full line) and curves simulated through eq. 15 with calibrated values of d_0 (dashed line) for specimens treated with WNC (black) and ANC (grey): a) Ajarte; b) Balegem; c) Obernkirchen; d) Schlaitdorf.

In order to better understand the physical meaning of the model, one has to focus on the interpretation of d_0. As previously discussed (§2.2), this parameter came out upon testing several trial functions to correlate the pore size to the reduced absorption rate: an exponential decay function of the type e^{-x/x_0} turned out to be the most suitable one. Exponential parameters like x_0, often referred to as characteristic constants, indicate how rapid the exponential decay is and, in this special case, d_0 contains information on the ability of the treatments to reduce the absorption rate of the stone pores. Since this parameter has the dimension of a length, it may be interpreted as representing a virtual pore whose absorption rate, according to the properties of the exponential function, is reduced to 37% after the application of the treatments. Pores with a larger diameter face a higher reduction, while smaller ones are less well protected. Actually, d_0 values obtained by linear regression (Table 6) always turn out to be lower than the smallest pore diameters measured in the MIP experiment (0.003 μm), so this virtual diameter does not refer to a real pore. However, in a qualitative sense, it may be associated to a threshold pore size that describes the extent to which the stone pores are protected after the application of the treatments: the lower this threshold is, the greater is the range of protected pores, going from the largest down to the smallest ones.

Table 6. Experimental values of sorptivity (C_{exp}, mg·cm^{-2}·s$^{-1/2}$) and amount of water absorbed per unit area at 96 h ($W_{f,exp}$, mg·cm^{-2}) for stones treated with WNC and ANC; values of sorptivity (C_{calc}) and amount of water absorbed per unit area at 96 h ($W_{f,calc}$) predicted by eq. 15; calibrated values of the exponential parameter d_0 (μm).

	Product	C_{exp}	$W_{f,exp}$	C_{calc}	$W_{f,calc}$	d_0
Ajarte	WNC	0.14	79	0.15	89	0.00074
	ANC	0.11	36	0.07	42	0.00055
Balegem	WNC	0.05	35	0.06	35	0.00178
	ANC	0.02	11	0.02	12	0.00115
Obernkirchen	WNC	0.08	33	0.06	36	0.00131
	ANC	0.08	18	0.03	20	0.00109

Schlaitdorf	WNC	0.13	52	0.09	51	0.00140
	ANC	0.09	24	0.05	27	0.00113

The relationship between the parameter d_0 and the protective performance of the treatments can be further explored by comparing d_0 values with those of relative sorptivity (C_t/C_{nt}). The trend shown in Figure 7 allows to observe that on each of the four stones, the treatment that is more effective in reducing the capillary uptake, ANC, is also the one with steadily lower values of d_0. This means that treatments with different penetration ability and protective effectiveness, when applied on the same stone substrate, can be discriminated on this basis.

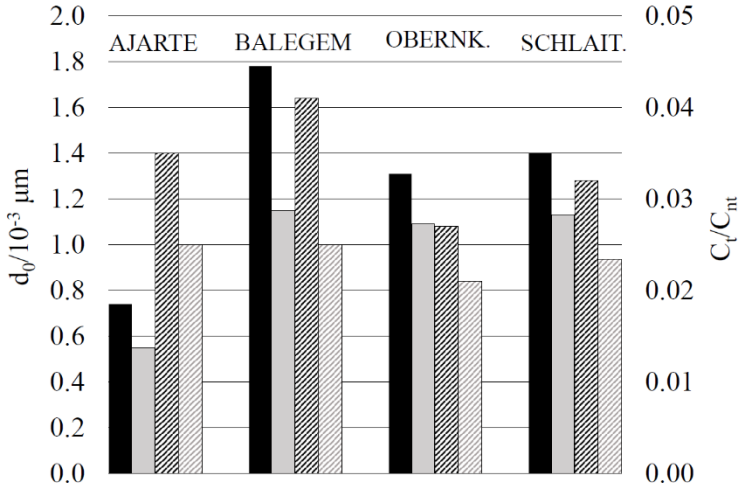

Figure 7. Comparison between d_0 values (full areas) and relative sorptivity (striped areas) of stone specimens treated with WNC (black) and ANC (grey).

Finally, the correlation of d_0 to the effective porosity P (eq. 20) in Figure 7b shows that the extent of pore hydrophobization also depends on the accessible porosity, which can be explained by the fact that the amount of treatments absorbed is strongly influenced by this parameter. The other factor is clearly represented by the properties of the products themselves, which are responsible for the distinct trends observed.

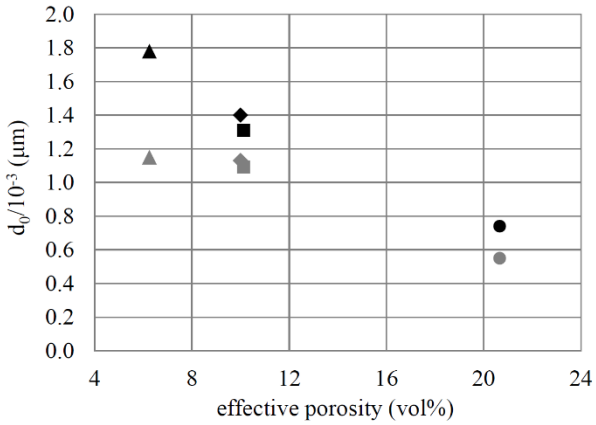

Figure 8. Correlation between the effective porosity of stones (P, vol%) and the corresponding d_0 value obtained by fitting eq. 15 to the experimental water absorption curves of specimens treated with WNC (black) and ANC (grey): Ajarte (●), Balegem (▲), Obernkirchen (■), Schlaitdorf (◆).

5. Conclusions

The predictive ability of two different models of capillary imbibition was tested on four natural stones and a large set of water absorption data, with the aim of validating an effective and easily implementable

methodology to simulate the hydric behaviour and calculate the sorptivity of porous ceramic materials used in historical architecture.

Both models showed the ability to provide fairly accurate predictions of materials sorptivity. Besides that, they are computationally very easy to handle and only require quite small samples (less than 1 cm^3) to obtain all the necessary input information (pore-size distribution and maximum water saturation) on the investigated materials, thus making a sustainable alternative to some of the current laboratory measurements (performed according to EN standard protocols) for the study of cultural heritage substrates, for which material sampling is often not allowed or subjected to strict limitations.

From a theoretical viewpoint, these models are based on two alternative descriptions of the stone microstructure, namely a capillary bundle and a pore network configuration, and use Lucas-Washburn equation to describe the imbibition dynamics. Although mercury intrusion porosimetry (MIP) is in either case the starting point, both models go substantially beyond the MIP-derived picture of the pore space, taking account of the fact that the arrangement and connectivity of the pores also affect the water absorption behaviour. MIP data such as the pore size distribution do not convey a definite microstructural configuration and, in the absence of a model of the pore space, they lead to the idea that pores may be regarded as an ensemble of independent, cylinder-like tubes. On such premises, the capillary uptake occurs through multiple imbibition fronts, since independent pores of different size must have different absorption rates. However, a general result of the present research was to show that a description of the capillary uptake based on multiple imbibition fronts fails to represent the kinetics of the process, leading to a substantial overestimation of sorptivity. Furthermore, the effective porosity, i.e., the fraction of pores that are actually involved in the imbibition process, may be significantly different from the MIP total open porosity. Both models overcome these issues by assuming a single imbibition front, which results from making proper assumptions on the topology of the pore space. Furthermore, by including an experimental term related to the maximum water saturation, they account for the non-complete filling of the pores due to local variations in capillary pressure and to the presence of residual air, which have fundamental importance in real imbibition processes.

Therefore, one first conclusion of the research was to show that the simple use of the MIP technique and its underlying conceptual framework cannot provide all the necessary microstructural information for describing the hydric behaviour of stones in a physically reasonable way. On the other hand, an approach combining MIP analysis, measurements of maximum water saturation and simple hypotheses on the geometry of the pore space allows to describe the imbibition process in small stone specimens with acceptable approximation and very little computational effort.

One second important result was to show that, if combined to a mechanistic model of pore hydrophobization, the proposed models of capillary imbibition are also able to account for the water absorption reduction that occurs in stone specimens after the application of protective treatments. This potentiality was tested on the same four natural stones after treating them with two innovative silicon-based products including a small fraction of titania nanoparticles. On each of the four stones, a correlation was observed between the extent of pore hydrophobization, as defined by the mechanistic model, and the reduction in sorptivity. Stone porosity and, in particular, the volume fraction of pores smaller than 1 μm turned out to be critical parameters for the performance of the products, controlling their penetration and distribution inside the porous matrix. This confirmed the basic assumption of the mechanistic model that small-size pores and stones having a significant fraction thereof are more difficult to protect.

Acknowledgements

The research received funding within the European programme Horizon 2020 (Nano-Cathedral Project: Nanomaterials for conservation of European architectural heritage developed by research on characteristic lithotypes, GA n. 646178). The Authors wish to thank Ms. Karin Fussenegger and Ms. Matea Ban from TU Wien for Mercury Intrusion Porosimetry measurements. Prof. Francesco Ballio and Prof. Giovanni Michele Porta from Politecnico di Milano are gratefully acknowledged for discussion and advice on the text.

References

[1] Doehne, E. (2002). Salt weathering: a selective review. *Geological society, London, special publications*, *205*(1), 51-64. https://doi.org/10.1144/GSL.SP.2002.205.01.05

[2] Scherer, G. W., & Valenza, J. J. (2005). Mechanisms of frost damage. In F. Young & J. P. Skalny (Eds.), *Materials science of concrete VII* (pp. 209-246). New York, NY: Wiley.

[3] Franzoni, E., & Sassoni, E. (2011). Correlation between microstructural characteristics and weight loss of natural stones exposed to simulated acid rain. *Science of the total environment*, *412*, 278-285. https://doi.org/10.1016/j.scitotenv.2011.09.080

[4] Ruedrich, J., Bartelsen, T., Dohrmann, R., & Siegesmund, S. (2011). Moisture expansion as a deterioration factor for sandstone used in buildings. *Environmental Earth Sciences*, *63*(7-8), 1545-1564. https://doi.org/10.1007/s12665-010-0767-0

[5] Franzoni, E., Sassoni, E., Scherer, G. W., & Naidu, S. (2013). Artificial weathering of stone by heating. *Journal of Cultural Heritage*, *14*(3), e85-e93. https://doi.org/10.1016/j.culher.2012.11.026

[6] Charola, A.E. (2001) Water repellents and other "protective" treatments: A critical review. In K. Littmann & A. E. Charola (Eds.), *Proceedings of Hydrophobe III - Third International Conference on Surface Technology with Water Repellent Agents* (pp. 3-19). Freiburg i. B., Germany: Aedificatio Verlag. Retrieved from http://hydrophobe.org/pdf/hannover/III_01.pdf

[7] EN 15801:2009. Conservation of Cultural Property—Test Methods—Determination of Water Absorption by Capillarity; European Committee for Standardization: Brussels, Belgium, 2009.

[8] Pia, G., Sassoni, E., Franzoni, E., & Sanna, U. (2014). Predicting capillary absorption of porous stones by a procedure based on an intermingled fractal units model. *International Journal of Engineering Science*, *82*, 196-204. https://doi.org/10.1016/j.ijengsci.2014.05.013

[9] De Buergo Ballester, M. A., & González, R. F. (2001). Basic methodology for the assessment and selection of water-repellent treatments applied on carbonatic materials. *Progress in Organic Coatings*, *43*(4), 258-266. https://doi.org/10.1016/S0300-9440(01)00204-1

[10] Gerdes, A., & Wittmann, F. H. (2003). Hydrophobieren von Stahlbeton, Teil 1: Transport und chemische Reaktionen silicium-organischer Verbindungen in der Betonrandzone. *International Journal for Restoration of Buildings and Monuments*, *9*, 41-64. Retrieved from https://www.researchgate.net/publication/262378014

[11] Bear, J. (1972). *Dynamics of fluids in porous media*. New York, NY: Dover Publications.

[12] Zimmerman, R. W., & Bodvarsson, G. S. (1989). An approximate solution for one-dimensional absorption in unsaturated porous media. *Water Resources Research*, *25*(6), 1422-1428. https://doi.org/10.1029/WR025i006p01422

[13] Dullien, F. A. L., El-Sayed, M. S., & Batra, V. K. (1977). Rate of capillary rise in porous media with nonuniform pores. *Journal of Colloid and Interface Science*, *60*(3), 497-506. https://doi.org/10.1016/0021-9797(77)90314-9

[14] Hammecker, C., Mertz, J. D., Fischer, C., & Jeannette, D. (1993). A geometrical model for numerical simulation of capillary imbibition in sedimentary rocks. *Transport in Porous Media*, *12*(2), 125-141. https://doi.org/10.1007/BF00616976

[15] Benavente, D., Lock, P., Del Cura, M. Á. G., & Ordóñez, S. (2002). Predicting the capillary imbibition of porous rocks from microstructure. *Transport in porous media*, *49*(1), 59-76. https://doi.org/10.1023/A:1016047122877

[16] Washburn, E. W. (1921). The dynamics of capillary flow. *Physical review*, *17*(3), 273. https://doi.org/10.1103/PhysRev.17.273

[17] Gladkikh, M., & Bryant, S. (2005). Prediction of imbibition in unconsolidated granular materials. *Journal of colloid and interface science*, *288*(2), 526-539. https://doi.org/10.1016/j.jcis.2005.03.029

[18] Dong, H., & Blunt, M. J. (2009). Pore-network extraction from micro-computerized-tomography images. *Physical review E*, *80*(3), 036307. https://doi.org/10.1103/PhysRevE.80.036307

[19] Pape, H., Clauser, C., & Iffland, J. (1999). Permeability prediction based on fractal pore-space geometry. *Geophysics*, *64*(5), 1447-1460. https://doi.org/10.1190/1.1444649

[20] Cai, J., & Yu, B. (2011). A discussion of the effect of tortuosity on the capillary imbibition in porous media. *Transport in Porous Media*, *89*(2), 251-263. https://doi.org/10.1007/s11242-011-9767-0

[21] Pia, G., & Sanna, U. (2014). An intermingled fractal units model and method to predict permeability in porous rock. *International Journal of Engineering Science*, *75*, 31-39. https://doi.org/10.1016/j.ijengsci.2013.11.002

[22] De Boever, W., Bultreys, T., Derluyn, H., Van Hoorebeke, L., & Cnudde, V. (2016). Comparison between traditional laboratory tests, permeability measurements and CT-based fluid flow modelling for cultural heritage applications. *Science of the Total Environment*, *554*, 102-112. https://doi.org/10.1016/j.scitotenv.2016.02.195

[23] Zhao, Y., Xue, S., Han, S., Chen, Z., Liu, S., Elsworth, D., & Chen, D. (2017). Effects of microstructure on water imbibition in sandstones using X-ray computed tomography and neutron radiography. *Journal of Geophysical Research: Solid Earth*, *122*(7), 4963-4981. https://doi.org/10.1002/2016JB013786
[24] Cnudde, V., Cnudde, J. P., Dupuis, C., & Jacobs, P. J. S. (2004). X-ray micro-CT used for the localization of water repellents and consolidants inside natural building stones. *Materials characterization*, *53*(2-4), 259-271. https://doi.org/10.1016/j.matchar.2004.08.011
[25] Casadio, F., & Toniolo, L. (2004). Polymer treatments for stone conservation: methods for evaluating penetration depth. *Journal of the American Institute for Conservation*, *43*(1), 3-21. https://doi.org/10.2307/3179848
[26] Maravelaki-Kalaitzaki, P., Kallithrakas-Kontos, N., Agioutantis, Z., Maurigiannakis, S., & Korakaki, D. (2008). A comparative study of porous limestones treated with silicon-based strengthening agents. *Progress in Organic Coatings*, *62*(1), 49-60. https://doi.org/10.1016/j.porgcoat.2007.09.020
[27] Pia, G., Corcione, C. E., Striani, R., Casnedi, L., & Sanna, U. (2017). Coating's influence on water vapour permeability of porous stones typically used in cultural heritage of Mediterranean area: Experimental tests and model controlling procedure. *Progress in Organic Coatings*, *102*, 239-246. https://doi.org/10.1016/j.porgcoat.2016.10.021
[28] Zoghlami, K., & Gómez-Gras, D. (2004). Determination of the distribution of consolidants and interpretation of mercury porosimetry data in a sandstone porous network using LSCM. *Microscopy research and technique*, *65*(6), 270-275. https://doi.org/10.1002/jemt.20119
[29] Mosquera, M. J., Pozo, J., Esquivias, L., Rivas, T., & Silva, B. (2002). Application of mercury porosimetry to the study of xerogels used as stone consolidants. *Journal of Non-Crystalline Solids*, *311*(2), 185-194. https://doi.org/10.1016/S0022-3093(02)01370-4
[30] Lazzeri, A., Coltelli, M. B., Castelvetro, V., Bianchi, S., Chiantore, O., Lezzerini, M., Niccolai, L., Weber, J., Rohatsch, A., Gherardi, F., & Toniolo, L. (2016). European Project NANO-CATHEDRAL: Nanomaterials for conservation of European architectural heritage developed by research on characteristic lithotypes. In J. Hughes & T. Howind (Eds.), *Science and Art: A Future for Stone: Proceedings of the 13th International Congress on the Deterioration and Conservation of Stone, Volume 1*. Paisley, United Kingdom: University of the West of Scotland.
[31] Lucas, R. (1918). Rate of capillary ascension of liquids. *Kolloid Zeitschrift*, *23*(15), 15-22. https://doi.org/10.1007/BF01461107
[32] Zhmud, B. V., Tiberg, F., & Hallstensson, K. (2000). Dynamics of capillary rise. *Journal of colloid and interface science*, *228*(2), 263-269. https://doi.org/10.1006/jcis.2000.6951
[33] Hamraoui, A., & Nylander, T. (2002). Analytical approach for the Lucas–Washburn equation. *Journal of colloid and interface science*, *250*(2), 415-421. https://doi.org/10.1006/jcis.2002.8288
[34] Siegesmund, S., & Dürrast, H. Physical and Mechanical Properties of Rocks. In: *Stone in architecture: properties, durability*, 5th ed., Siegesmund, S., Snethlage, R., Eds.; Springer Verlag, Berlin-Heidelberg, Germany, 2014; pp. 97-224. https://doi.org/10.1007/978-3-642-45155-3_3
[35] Fries, N., & Dreyer, M. (2008). An analytic solution of capillary rise restrained by gravity. *Journal of colloid and interface science*, *320*(1), 259-263. https://doi.org/10.1016/j.jcis.2008.01.009
[36] Lavi, B., Marmur, A., & Bachmann, J. (2008). Porous media characterization by the two-liquid method: effect of dynamic contact angle and inertia. *Langmuir*, *24*(5), 1918-1923. https://doi.org/10.1021/la702090x
[37] Cai, J., Yu, B., Zou, M., & Luo, L. (2010). Fractal characterization of spontaneous co-current imbibition in porous media. *Energy & Fuels*, *24*(3), 1860-1867. https://doi.org/10.1021/ef901413p
[38] Handy, L. L. (1960). Determination of effective capillary pressures for porous media from imbibition data. *Petroleum Transactions AIME*, *219*, 75-80.
[39] Li, K., & Horne, R. N. (2004). An analytical scaling method for spontaneous imbibition in gas/water/rock systems. *SPE Journal*, *9*(03), 322-329. https://doi.org/10.2118/88996-PA
[40] Cai, J., Perfect, E., Cheng, C. L., & Hu, X. (2014). Generalized modeling of spontaneous imbibition based on Hagen–Poiseuille flow in tortuous capillaries with variably shaped apertures. *Langmuir*, *30*(18), 5142-5151. https://doi.org/10.1021/la5007204
[41] Yu, B., & Li, J. (2001). Some fractal characters of porous media. Fractals, 9(03), 365-372. https://doi.org/10.1142/S0218348X01000804
[42] Yu, B., & Cheng, P. (2002). A fractal permeability model for bi-dispersed porous media. *International Journal of Heat and Mass Transfer*, *45*(14), 2983-2993. https://doi.org/10.1016/S0017-9310(02)00014-5

[43] Bo-Ming, Y. (2005). Fractal character for tortuous streamtubes in porous media. *Chinese Physics Letters*, *22*(1), 158. https://doi.org/10.1088/0256-307X/22/1/045
[44] Xu, P., & Yu, B. (2008). Developing a new form of permeability and Kozeny–Carman constant for homogeneous porous media by means of fractal geometry. *Advances in water resources*, *31*(1), 74-81. https://doi.org/10.1016/j.advwatres.2007.06.003
[45] Comiti, J., & Renaud, M. (1989). A new model for determining mean structure parameters of fixed beds from pressure drop measurements: application to beds packed with parallelepipedal particles. *Chemical Engineering Science*, *44*(7), 1539-1545. https://doi.org/10.1016/0009-2509(89)80031-4
[46] Kontogeorgos, D. A., & Founti, M. A. (2013). A generalized methodology for the definition of reactive porous materials physical properties: Prediction of gypsum board properties. *Construction and Building Materials*, *48*, 804-813. https://doi.org/10.1016/j.conbuildmat.2013.07.095
[47] Nonweiler, T. R. F. (1975). Flow of biological fluids through non-ideal capillaries. *Encyclopedia of Plant Physiology*, *1*, 474-477.
[48] Kirkpatrick, S. (1973). Percolation and conduction. *Reviews of modern physics*, *45*(4), 574-588. https://doi.org/10.1103/RevModPhys.45.574
[49] Guryev, V. V., Nikitsin, V. I., & Kofanov, V. A. (2016). Determination of the hydraulic radius of the porous structure of ceramic materials. *Glass and Ceramics*, *73*(7-8), 258-265. https://doi.org/10.1007/s10717-016-9869-9
[50] Lezzerini, M., Marroni, M., Raneri, S., Tamayo, S., Narbona, B., Fernández, B., Weber, J., Ghaffari, E., Ban, M., & Rohatsch, A. (2017). D1.5 – Mapping of stones and their decay: Part I - Natural stone test methods, NanoCathedral project Grant Agreement no. 646178 - confidential deliverable (pp. 8-16).
[51] ISO 15901-1:2016. Evaluation of pore size distribution and porosity of solid materials by mercury porosimetry and gas adsorption—Part 1: Mercury porosimetry; International Organization for Standardization: Geneva, Switzerland, 2016.
[52] EN 13755:2008. Natural stone test methods - Determination of water absorption at atmospheric pressure; European Committee for Standardization: Brussels, Belgium, 2008.
[53] Gherardi, F., Roveri, M., Goidanich, S., & Toniolo, L. (2018). Photocatalytic nanocomposites for the protection of European architectural heritage. *Materials*, 11(1), 65. https://doi.org/10.3390/ma11010065
[54] Roveri, M., Gherardi, F., Brambilla, L., Castiglioni, C., & Toniolo, L. (2018). Stone/coating interaction and durability of Si-based photocatalytic nanocomposites applied to porous lithotypes. *Materials*, 11(11), 2289. https://doi.org/10.3390/ma11112289
[55] Chitsazian, H. A. (1985). Beziehungen zwischen Mineralbestand, Gefüge und technologischen Eigenschaften der Niedersächsischen" Wealden"-Sandsteine (Unterkreide). In *Mitteilungen aus dem Geologischen Institut der Universität Hannover, Heft 25* (pp. 1-103). Hannover, Germany: Universität Hannover. Institut für Geologie und Paläontologie. Retrieved from https://www.repo.uni-hannover.de/handle/123456789/457
[56] Akin, S., Schembre, J. M., Bhat, S. K., & Kovscek, A. R. (2000). Spontaneous imbibition characteristics of diatomite. *Journal of Petroleum Science and Engineering*, *25*(3-4), 149-165. https://doi.org/10.1016/S0920-4105(00)00010-3
[57] Kang, M., Perfect, E., Cheng, C. L., Bilheux, H. Z., Gragg, M., Wright, D. M., & Warren, J. M. (2013). Diffusivity and sorptivity of Berea sandstone determined using neutron radiography. *Vadose Zone Journal*, *12*(3). https://doi.org/10.2136/vzj2012.0135
[58] Raimondo, M., Dondi, M., Gardini, D., Guarini, G., & Mazzanti, F. (2009). Predicting the initial rate of water absorption in clay bricks. *Construction and Building Materials*, *23*(7), 2623-2630. https://doi.org/10.1016/j.conbuildmat.2009.01.009
[59] Koponen, A., Kataja, M., & Timonen, J. (1996). Tortuous flow in porous media. *Physical Review E*, *54*(1), 406-410. https://doi.org/10.1103/PhysRevE.54.406
[60] Mota, M., Teixeira, J. A., Bowen, W. R., & Yelshin, A. (2001). Binary spherical particle mixed beds: porosity and permeability relationship measurement. *Transactions of the Filtration Society*, *1*(4), 101-106. Retrived from https://repositorium.sdum.uminho.pt/bitstream/1822/1403/1/2001-17%5b1%5d.pdf
[61] Matyka, M., Khalili, A., & Koza, Z. (2008). Tortuosity-porosity relation in porous media flow. *Physical Review E*, *78*(2), 026306. https://doi.org/10.1103/PhysRevE.78.026306
[62] Beltrán, V., Escardino, A., Feliu, C., Rodrigo, M.D. (1988). Liquid suction by porous ceramic materials. *British ceramic. Transactions and journal*, *87*(2), 64-69.